Methods for quantifying methane emissions using unmanned aerial vehicles: A review

Jacob T. Shaw, Adil Shah, Han Yong, Grant Allen

Review

Authors for correspondence:
Jacob T. Shaw
e-mail: jacob.shaw@manchester.ac.uk
Grant Allen
e-mail: grant.allen@manchester.ac.uk

Methods for quantifying methane emissions using unmanned aerial vehicles: a review

Jacob T. Shaw[1], Adil Shah[2], Han Yong[1] and Grant Allen[1]

[1]Centre for Atmospheric Science, Department of Earth and Environmental Science, University of Manchester, Manchester, UK
[2]Laboratoire des Sciences du Climat et de l'Environnement (LSCE), CEA CNRS, UVSQ UPSACLAY, Gif sur Yvette, France

JTS, 0000-0003-3558-3894; AS, 0000-0002-5692-3715; GA, 0000-0002-7070-3620

Methane is an important greenhouse gas, emissions of which have vital consequences for global climate change. Understanding and quantifying the sources (and sinks) of atmospheric methane is integral for climate change mitigation and emission reduction strategies, such as those outlined in the 2015 UN Paris Agreement on Climate Change. There are ongoing international efforts to constrain the global methane budget, using a wide variety of measurement platforms across a range of spatial and temporal scales. The advancements in unmanned aerial vehicle (UAV) technology over the past decade have opened up a new avenue for methane emission quantification. UAVs can be uniquely equipped to monitor natural and anthropogenic emissions at local scales, displaying clear advantages in versatility and manoeuvrability relative to other platforms. Their use is not without challenge, however: further miniaturization of high-performance methane instrumentation is needed to fully use the benefits UAVs afford. Developments in the models used to simulate atmospheric transport and dispersion across small, local scales are also crucial to improved flux accuracy and precision. This paper aims to provide an overview of currently available

UAV-based technologies and sampling methodologies which can be used to quantify methane emission fluxes at local scales.

This article is part of a discussion meeting issue 'Rising methane: is warming feeding warming? (part 1)'.

1. Introduction

Understanding and quantifying the global methane (CH_4) budget is crucial for the prediction and mitigation of future climate change. Both emissions of CH_4 to atmosphere and the absolute concentration of CH_4 in the atmosphere have increased over the past decade [1], and there are concerns that climate feedbacks are further increasing emissions from natural sources [2]. Quantification of methane emissions at local scales (defined for the purposes of this review to be less than 1 km) is important for understanding natural methane production and emission processes, and also for informing emission reduction strategies and regulation for anthropogenic methane sources [2,3]. Emission flux quantification generally relies on either bottom-up, or top-down, methodologies, and validation of inventories requires a comparison of both approaches. Bottom-up inventories combine data-driven emission factors with statistical activity data, or use process-based modelling, whereas top-down methods combine atmospheric sampling with atmospheric advection (or dispersion) models to derive emission fluxes. Bottom-up estimates of the global methane budget (750 Tg yr^{-1} for 2017) are approximately 30% larger than equivalent top-down estimates (600 Tg yr^{-1} for 2017) [4]. There is therefore a need to reconcile and validate bottom-up emission inventory estimates and process-based models with top-down (measurement based) methodology.

Typically, quantifying methane emission fluxes requires the continuous sampling of atmospheric winds, coupled to absolute methane mole fraction measurements. Unfortunately, practical constraints typically require compromises to be made in both the temporal range and spatial resolution of measurements. Put simply, sampling methods cannot measure everywhere, all of the time. The empirical measurement data must typically be interpolated, assimilated or extrapolated, often by making use of models which simulate atmospheric dispersion and transport. All such flux quantification methods have intrinsic uncertainties and assumptions, many associated with the highly challenging simulation of atmospheric circulation, and assumptions therein.

A variety of platforms for the measurement of methane exist. These can range from ground-based systems (e.g. [5]), to instrumentation fitted onboard aircraft (e.g. [6–10]), to satellites, which monitor total atmospheric-column methane from low-Earth orbit (e.g. [11–13]). Measurement platforms can be geospatially fixed, in the form of towers (e.g. [14]) or long-term fixed-site monitoring stations (e.g. [15]), or geospatially flexible, in a moving vehicle for example (e.g. [16–18]). However, there remains a substantial sampling void between the ground, and altitudes of up to 100 m above ground, in which mobile platforms have been unable to operate until recently.

Large research aircraft lack the manoeuvrability to suitably sample methane emissions from small, local sources such as landfill or fossil fuel extraction facilities. Instead, large aircraft are more suited to regional-scale emissions quantification, such as those from wetlands or from cities, where they are not limited by their rapid speed or by flight restrictions (e.g. [19–21]). Lighter manned-aircraft have been used to measure fluxes from small, local sources, but typically require conditions including a stable background and an absence of significant extraneous sources (e.g. [22,23]). Such conditions are often found over the ocean, where manned-aircraft may also benefit from reduced flight restrictions compared with over land.

Unmanned (or uncrewed) aerial vehicles (UAVs; sometimes unmanned aerial systems or remotely piloted aerial systems), colloquially referred to as drones, offer a flexible monitoring

platform for *in situ* atmospheric measurements or remote sensing of methane concentrations at the spatial scale of local sources (less than 1 km) and small facilities. UAVs can be equipped to dynamically monitor the lower atmosphere and planetary boundary layer (e.g. [24]) within the limits of local flight restrictions, and consequently their use and versatility in atmospheric measurement has expanded considerably in the past decade (e.g. [25–28]). The advent of small (but relatively imprecise) trace gas sensors has also reduced the cost of operating UAV monitoring platforms to near-consumable levels. UAVs are also uniquely placed for monitoring in hazardous, remote or difficult-to-access environments (e.g. [29,30]). Here, we review methods and approaches for quantifying methane emission fluxes which make use of UAVs as a measurement platform, focusing in particular on small UAVs with a maximum take-off weight of less than approximately 20 kg. UAVs below this mass are typically subject to reduced regulation; however, it should be noted that law and regulation varies considerably internationally. Regulatory standards will not be debated further in this review. We also do not review large remote-piloted UAVs (which are often used for military applications). Small UAVs are generally limited to operating at altitudes below 1 km and have shorter flight durations, making them ideally suited for trace gas detection in the near-surface atmospheric boundary layer [31,32]. The methods discussed within this review are most applicable to the characterization of methane emissions from localized- and facility-scale emission sources, be they natural or anthropogenic in nature.

2. Unmanned aerial vehicle platforms

There are many different makes and types of small UAV platform available on the commercial market, with an expansive range of specifications, including weight, payload limit, maximum air speed, wing type and propeller type. The choice of UAV platform will not be discussed here in detail. Recent and comprehensive reviews of UAV platforms already exist (e.g. [31,32]). An example selection of UAV platforms previously used for methane detection and measurement is shown in figure 1. Small UAVs vary in mass on a scale from 100 g (micro-UAVs) through to 20 kg (and heavier), with implications for payload capacity and flight endurance. The UAVs can be powered by liquid fuel, but batteries are increasingly popular. Most small UAVs are limited to maximum air speeds of $15 \, \text{m s}^{-1}$, although this typically decreases during strong winds, and with increased UAV payload. Heavy payloads can also reduce flight endurance; small UAVs are typically limited to approximately 30 min of flight time, depending on sampling strategy, and the strength of the winds. Additional batteries (or liquid fuel) can be used to improve flight endurance, but only up to a threshold, where the weight of additional fuel becomes a burden. It should be noted that UAV platform specifications vary considerably, and that the values stated here are only representative of small UAVs at the time of writing. Technology continues to improve in regards to many of these aspects.

Aside from classifications based on size and payload weight, UAVs can be broadly divided into fixed-wing and rotary-wing aircraft. Fixed-wing UAVs resemble traditional airplanes and the largest of these (e.g. NASA Global Hawk [31]) can benefit from enhanced stability (especially in more challenging weather conditions) and often an increased payload capability relative to rotary-wing UAVs [32]. However, small fixed-wing UAVs typically suffer from the same limitations as rotary-wing UAVs, in terms of stability and payload capacity. Small rotary-wing UAVs do have greater manoeuvrability and are able to perform vertical take-off and landing procedures, which offers practical advantages for fieldwork. Whereas small fixed-wing UAVs are typically faster and can sample across a greater spatial area in a shorter period of time. Both types of UAV have been used for trace gas detection and flux quantification. In summary, care must be taken when selecting a UAV platform, and consideration as to the exact application and intended operational environment should be made before purchase.
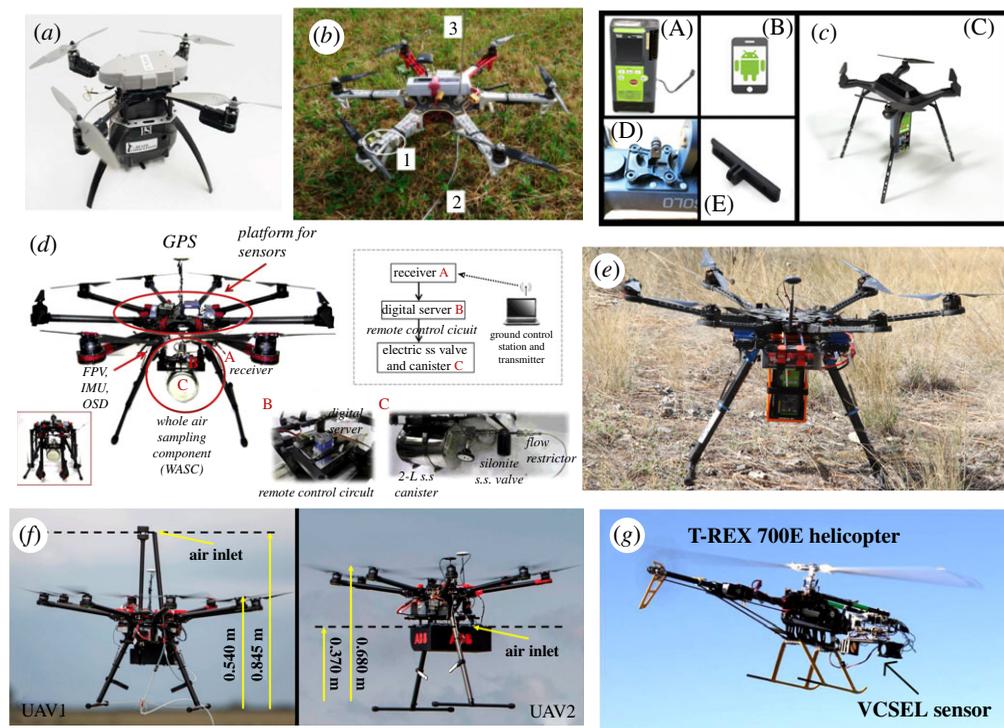
Figure 1. Selected examples showing UAV platforms and methane instrumentation from the literature. (*a*) The *Remote Methane Leak Detector* quadrotor UAV. Image from Yang *et al*. [33]. (*b*) A DJI F550 multicopter with installed sensors and tubing. Image from Brosy *et al*. [34]. (*c*) 3DR Solo quadrotor UAV and methane sensor. Image from Oberle *et al*. [35]. (*d*) Octorotor multicopter with a whole air sampling system and multiple environmental sensors attached. Image from Chang *et al*. [36]. (*e*) A hexacopter UAV with laser-based methane detector attached. Image from Emran *et al*. [37]. (*f*) Two adapted DJI Spreading Wings S1000 + octorotor multicopter UAVs—the left-hand UAV shows Teflon tubing to a ground-based instrument and the right-hand UAV has methane sensor attached. Image from Shah *et al*. [38]. (*g*) T-REX 700E robotic helicopter with methane sensor. Image from Khan *et al*. [39]. (Online version in colour.)

3. Wind measurement approaches

Accurate wind speed and wind direction is typically required for flux quantification. These can be measured (or inferred) from a suitable nearby monitoring station, equipped with anemometer instrumentation, but doing so may introduce some measure of uncertainty [40]. Preferably, the wind vector should be measured from onboard the UAV platform, and at a high spatial and temporal resolution, matching, if not exceeding, that of the methane measurement sampling rate. However, care must be taken to avoid interference of the wind field by the UAV platform itself. This is a particular challenge for rotary-wing UAVs, as the propellers constitute a barrier to ambient flow.

Various sensors for measuring wind velocity onboard a UAV already exist; multi-hole pressure sensors [41–43], or Pitot-tubes [44,45], are suited to fixed-wing UAVs. It is also possible to derive mean wind speed values in the absence of a designated sensor, through the use of a global navigation satellite system to infer wind speed from the ground speed and flight path bearing [46,47], using knowledge of the inertia of the UAV. Elston *et al*. [48] provide an overview of different types of wind sensors, and their applicability for fixed-wing platforms, and Rautenberg *et al*. [49] compare a number of different algorithms for the calculation of wind speed and wind direction against direct three-dimensional wind vector measurements. A five-hole probe mounted on a fixed-wing UAV has been observed to perform poorly for wind measurements when compared with measurements from a ground-based static sonic anemometer [40].

More recently, deriving wind measurements onboard rotary-wing UAVs has become possible [50]. This is traditionally considered more difficult due to strong perturbations in the wind flow induced by the rotating propellers, but results have been promising, with uncertainties below $0.5 \, \mathrm{m \, s^{-1}}$ for wind speed, and 30° for wind direction [51]. Barbieri *et al.* [52] assessed 38 different UAV platforms carrying 23 unique two- and three-dimensional anemometers against reference measurements made from a meteorological tower and found that sonic anemometers mounted on rotary-wing UAVs provided the most accurate wind field measurements. However, while horizontal winds may be measurable using sonic anemometers on rotary-wing UAVs, three-dimensional (turbulence-scale) winds are far more problematic due to vertical flow disturbance by propellers. Mounting such sensors away from the plane of the propellers may overcome this, but the induced moment of adding mass away from the centre of gravity can significantly impact flight duration and lead to platform instability and oscillations.

4. Methane measurement approaches

A broad range of instrumentation for the measurement of methane exists, some of which may be more, or less, applicable for mounting onto a UAV platform [53,54]. Methane instrumentation applicable for small UAVs display a diverse variety of specifications, including measurement type, weight, measurement frequency, detection limit and precision (e.g. [55–58]). Some of these parameters, such as the instrument response time, will have an impact on the accuracy and spatio-temporal representability of measurements when using a mobile platform [59]. Instruments that offer excellent performance in terms of measurement sensitivity and precision have long been available, but these are generally more suitable for manned-aircraft (e.g. [7]), or ground-based applications (e.g. [15]), where there are fewer constraints on size, weight and power consumption (as well as cost).

UAV-based methane measurements have generally been made using three different methods, each with their own individual advantages and disadvantages [60].

1. *Air samples collected onboard the UAV.* Air samples are collected for later offline (laboratory-based) analysis of the methane mole fraction (e.g. [36,61–64]). This method can make use of the high-performance instrumentation (operated in the laboratory using the collected air samples) but usually results in discretized (snapshot), rather than continuous, spatially varying methane measurements. AirCore systems can be used for continuous atmospheric sampling but this typically results in low spatial resolution (greater than 20 m), even when sampling at air speeds below $2 \, \mathrm{m \, s^{-1}}$ [63]. Additionally, offline analysis allows for the easy measurement of other variables, such as the ^{13}C isotopic ratio of the methane, or other atmospheric trace gases (which may greatly aid source apportionment) assuming that chemical ageing of the sample has not taken place post-collection.

2. *Air sampled through tubing connected to the UAV.* Air is sampled through a tube (often referred to as a tether) carried by the UAV and measured by an instrument on the ground (e.g. [34,38,65] and figure 2). This method allows for the beneficial use of high-performance ground-based instrumentation which would otherwise be impossible for a UAV to carry, and which can also be operated continuously. Care must be taken to convolve the sampling time with the actual sampling location by accounting for the lag-time through the tubing, which can be on the order of 100 m in length. The use of a tether can also present logistical challenges, such as kinking of the tubing, or snaring on obstacles. A tether also limits a UAVs manoeuvrability and reduces both its horizontal and vertical range of motion and introduces flight hazards that may need to be mitigated.

3. *Air sampled live onboard the UAV.* This is perhaps the optimal method, but requires a sufficiently lightweight instrument, which can have consequences for both the precision of, and the resolution of, measurements. Onboard instrumentation allows the UAV full spatial freedom, but added weight may substantially impact flight duration. While
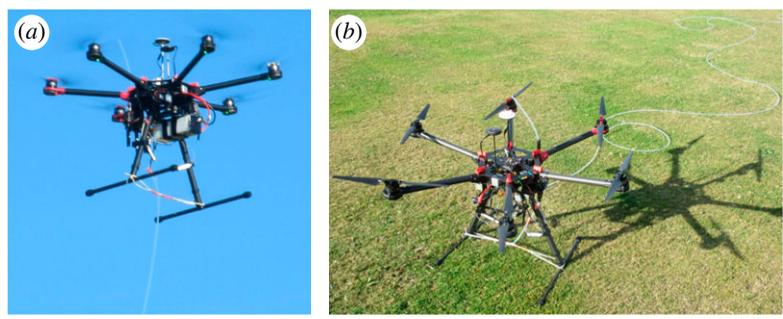
Figure 2. (*a*) A DJI Spreading Wings S900 UAV in flight; (*b*) The same UAV on the ground, with a 150 m long Teflon tether, connected to a methane instrument on the ground (not shown). Note that the tether is connected to an air inlet above the plane of the propellers. Image taken from Shah *et al.* [66]. (Online version in colour.)

lightweight but limited-performance methane sensors already exist (e.g. [67]), high-precision instrumentation less than 5 kg in weight are only just becoming commercially available. Rapid advances in the miniaturization of such instruments continue to be made, and instruments are known to be in development by various commercial manufacturers.

Many currently available lightweight methane sensors employ near-infrared laser sources. For example, Gardiner *et al.* [68] demonstrated a near-infrared tunable diode laser absorption spectrometer for methane detection (6 kg, ±10% precision). Near-infrared sensors have been used to successfully map landfill methane hot spots from a rotary-wing UAV [69]. Mid-infrared laser sources make use of stronger methane absorption lines than near-infrared laser sources [55]. Golston *et al.* [70] presented a lightweight, mid-infrared methane sensor, with two designs weighing 1.6 and 4.6 kg, demonstrating 10 and 5 ppb precision at 1 Hz, respectively.

Non-dispersive infrared sensors have shown poor methane precision (±1160 ppb at 1 Hz) on UAVs, suggesting that they may be unable to quantify methane emission fluxes on the order of $1 \, g \, s^{-1}$ at local scales [67]. Non-dispersive sensors may have applications in the detection of large methane mole fraction enhancements (of at least 10 ppm) and should, like any new instrumentation, be rigorously characterized and tested for accuracy, precision and drift before use in scientific applications [67].

Open-path, tunable diode laser-based sensors can provide precise and fast measurements and are relatively lightweight [53,71]. Emran *et al.* [37] attached an open-path methane sensor (0.6 kg ± 10% precision), operating at 10 Hz, to their rotary-wing UAV. The same methane sensor was used to map the spatial distribution of methane over Arctic permafrost from a rotary-wing UAV, albeit with a methane concentration uncertainty of ±40% after calibration [35]. Nathan *et al.* [71] used a 3.1 kg open-path instrument to measure methane at 1 Hz, with a precision of approximately ±100 ppb. A miniaturized sensor (0.25 kg), based on technology built for the Mars Curiosity Rover, was used to detect controlled emissions of methane with ±10 ppb sensitivity at 1 Hz, but with potentially many hundreds ppb drift due to internal thermal changes [72]. Natural gas leaks were successfully detected using an open-path tunable laser diode absorption spectrometer attached to a fixed-wing UAV, with 90 min of flight time [73]. However, the instrument displayed substantial noise error in the field (up to 1.0 ppm), and there was only a 20% chance of successful leak detection, even when surveying large controlled emission rates [74]. An alternative open-path method used a dual-frequency-comb telescope on the ground, with an airborne retroreflector aboard a rotary-wing UAV, to measure methane, with a precision of ±6 ppb [75]. This method avoids the limitations resulting from mounting typically heavy instrumentation, while maintaining the advantages of flexible UAV-based spatial sampling [75].

Cavity-based laser absorption instrumentation typically offers higher precision measurements but tend to require more specialist operation and expertise than open-path technology. A low-power vertical cavity surface-emitting laser (2 kg) was tested aboard a robotic helicopter; results demonstrated a ±1% precision and also a long-term drift in methane measurements of around 1% [39]. Berman *et al*. [76] used a 19.5 kg off-axis integrated cavity output spectrometer with an 8 h battery life onboard a fixed-wing UAV to measure methane mole fraction in the Arctic. Laboratory testing demonstrated a precision of ±2.0 ppb (1σ) methane over an atmospherically relevant range of mole fractions, albeit with a small interference due to temperature [76]. Such a heavy payload will only be useful when using larger, sturdier UAVs with maximum take-off weights greater than 20 kg, however. A prototype of a miniaturized off-axis integrated cavity output spectrometer (3.4 kg, 32 W, 2 ppb at 1 Hz precision) built specifically for UAV use was tested on a rotary-wing UAV and successfully used to calculate methane fluxes [38,65]. Similarly, an open-path cavity ring-down spectroscopy instrument (4.1 kg) was successfully integrated onboard a rotary-wing UAV, demonstrating in-flight precisions of between 10 and 30 ppb [77]. This platform was used to monitor isolated plumes from controlled releases of methane of $0.5\,\mathrm{g\,s^{-1}}$ [77]. Elsewhere, a ground-based cavity ring-down spectrometer was tethered to a rotary-wing UAV, providing stable methane measurements with a precision of ±7 ppb [34]. The 50 m length of tubing, attached to an inlet 30 cm above the UAV propellers, gave an additional payload weight of just 0.65 kg. Results showed good agreement between the UAV-based and adjacent tower-based methane mole fraction measurements [34].

Additionally, methane emissions can be detected qualitatively using thermal imaging. This is particularly useful for leak detection, but not for flux quantification, without additional supporting measurements. Tratt *et al*. [78] used airborne thermal-infrared hyperspectral imaging spectrometry to visualize methane emissions from various fossil fuel sources while Lehmann *et al*. [79] used high-resolution colour infrared images to map methane hot spots and upscale independent chamber-derived methane emission fluxes in a natural peat bog ecosystem. Tanda *et al*. [80] used airborne infrared thermography to detect methane emissions from landfill and were able to provide a crude estimate of methane flux rate using a simple relationship between observed heat exchange and the heat associated with methane production. Similarly, a UAV-mounted thermal-infrared camera was used to visualize methane emissions from a Danish landfill, but methane flux was quantified more rigorously using independent surface chamber measurements [81]. Three different imaging sensors (RGB, thermal-infrared and near-infrared), mounted on a rotary-wing UAV, were compared for their applicability for mapping landfill emissions in Lithuania [82].

Non-optical approaches have also been tested for UAV-mounted applicability. Solid-state, or chemical, sensors offer a low-cost, low-weight alternative to typically bulky and technologically expensive laser-based systems (e.g. [83,84]). Taguem *et al*. [85] tested a series of metal oxide sensors in the laboratory for the purpose of UAV-mounted monitoring, but did not report any operational flight data. Despite reporting a linear response between sensor readings and methane concentration, Taguem *et al*. [85] concluded that in-field sampling may be difficult due to low sensitivity to methane and sensor response to other trace gases. Ali *et al*. [86] used a semiconductor-based methane sensor for their UAV-based measurements, albeit with a high limit of detection (10 ppm) which may only be suitable for sampling methane very close to emission sources.

A summary of the methane instrumentation that has been deployed on UAV platforms is presented in table 1.

5. Methane flux quantification

A variety of methods have been used to quantify methane emission fluxes from many emission sources. Here, we review many of the techniques that have been applied to UAV-based measurements.

Table 1. Summary of methane instrumentation deployed on UAV platforms.

measurement type	mass (kg)	power consumption (W)	precision	resolution (Hz)	notes	reference
off-axis integrated cavity output spectroscopy	19.5 (with ancillary systems)	70	2 ppb (in laboratory)	1	temperature interference	[76]
mid-infrared open-path wavelength modulated spectroscopy	4.6 1.6	30	5 ppb 10 ppb	1–10		[70,87]
handheld open-path	0.6		10%	10	path-averaged concentration	[35,37]
near-infrared standoff tunable diode laser absorption spectroscopy	1.4	1			path-averaged concentration	[69]
custom open-path	3.1	25	100 ppb or 10%	1	path-averaged concentration	[71]
near-infrared vertical cavity surface-emitting laser	2	2	1%	1	long-term drift around 1%	[39]
near-infrared tunable diode laser absorption spectroscopy	6		10%	0.5		[68]
tunable laser spectroscopy	0.25		10 ppb	1	potentially 100 s ppb drift due to thermal interference	[72]
open-path cavity ring-down spectroscopy	4.1	12	5–10 ppb (in laboratory) 10–30 ppb (in field)	1		[77]
open-path tunable laser diode spectroscopy					noise on the order of 1000 ppb; path-averaged concentration	[73,74]

(*Continued.*)

8

royalsocietypublishing.org/journal/rsta *Phil. Trans. R. Soc. A* **379**: 20200450

Table 1. (Continued.)

measurement type	mass (kg)	power consumption (W)	precision	resolution (Hz)	notes	reference
non-dispersive infrared	1.5 (with ancillary systems)	4.2	1160 ppb	1		[67]
dual-frequency-comb telescope (ground-based)	N/A		16 ppb	0.1	UAV carried an airborne retroreflector path-averaged concentration	[75]
off-axis integrated cavity output spectroscopy (tethered)	N/A	35	0.7 ppb @ 1 Hz	10		[38,65]
off-axis integrated cavity output spectroscopy	3.4	32	2 ppb @ 1 Hz	5		[38,65]
cavity ring-down spectroscopy (tethered)	N/A		7 ppb			[34]

(a) Mass balance box modelling

Mass balance (or mass budget) box methods consider the conservation of the mass of methane within a system (or volume), usually conceptualized as a box. This method has been routinely used in manned-aircraft-based flux quantification, for deriving methane emission fluxes from cities (e.g. [20,88]), from wetlands [19] and from industrial regions (e.g. [6,21]). The emission flux is typically quantified as demonstrated by equation (5.1):

$$F = \int_{z_1}^{z_2} \int_{x_1}^{x_2} ([CH_4] - [CH_4]_b) U_\perp \, dx dz, \quad (5.1)$$

where F is the emission flux, and the enhancement of methane is quantified by subtracting the 'background' methane concentration ($[CH_4]_b$; usually measured upwind of the source) from measurements of methane within the emission plume ($[CH_4]$) [89]. $U_\perp$ is the wind speed perpendicular to the vertical plane upon which the plume is projected. These values are integrated over both the horizontal extent (between x_1 and x_2), and the vertical extent (between z_1 and z_2), of the emission plume. It should be noted that in order to derive a flux in units of mass per unit time ($g\,s^{-1}$ for example), many direct methane concentration measurements will need to be converted from the mole fraction (in ppb or ppm) typically recorded by many instruments, to a mass density (in $g\,m^{-3}$ for example).

The mass balance method generally requires that the wind field is constant between upwind and downwind measurements, i.e. that the wind speed and wind direction does not change. However, wind field variability can be implicitly accounted for through robust uncertainty propagation [8]. When using manned-aircraft for sampling, the atmosphere is usually considered to be vertically well-mixed, and this may be the case if measurements are made sufficiently downwind of the emission source. If this cannot be assumed, then the vertical variability in methane must be either measured, approximated or both [90]. For UAV-based sampling, where measurements can be made much closer to the source, the plume is unlikely to be vertically well-mixed, but dense spatial sampling is still important for flux accuracy [71].

Allen *et al.* [40] used the mass balance method, in conjunction with UAV-based measurements of CH_4 and CO_2 to quantify a methane flux from landfill. They used two UAV platforms: a fixed-wing UAV equipped with a high-precision CO_2 instrument (non-dispersive infrared, 0.3 kg, 1% precision at 1 Hz sampling rate) and a rotary-wing UAV tethered to an off-axis Integrated Cavity Output Spectrometer (ICOS; Los Gatos Research (now ABB) Ultraportable Greenhouse Gas Analyzer [91]). The rotary-wing UAV was used to determine the vertical mixing of methane and CO_2, while the fixed-wing UAV was used for horizontal measurements of CO_2, from which the horizontal distribution of methane was inferred using emission ratios characteristic of landfills (figure 3). Methane fluxes were quantified for two flights (0.14 ± 0.09 and $0.05 \pm 0.03\,kg\,s^{-1}$) with the uncertainties mainly influenced by the variability in the methane background, and the variability in the wind. Their reported uncertainties were comparable to uncertainties derived from other non-UAV-based landfill flux estimation methods (e.g. [92]). However, CO_2 can be a poor proxy for landfill methane emissions in the presence of interfering (off-site) sources [60] and the use of a dedicated methane instrument on both UAVs would have been preferable [40].

Nathan *et al.* [71] used the mass balance method to estimate the methane emission rate from a compressor station. They deployed an open-path methane sensor (3.1 kg, 10 Hz, 100 ppb precision) on a fixed-wing UAV. Kriging (e.g. [20,93]) was used to interpolate between the spatially sparse measurements on the two-dimensional vertical sampling plane. The mean methane emission flux from 22 flights was estimated to be $14 \pm 8\,g\,s^{-1}$. This was larger than the fluxes quantified by two additional, non-UAV-based methods, which yielded methane emission rates of $5.8\,g\,s^{-1}$. Nathan *et al.* [71] noted that their method was limited by the low density of their spatial sampling and found potential biases resulting from the emission plume centre changing over time. The variability in the plume morphology, distinguished as an instantaneous plume as opposed to a time-averaged plume, means that there are problems with using interpolation methods (such as kriging) to infer the spatial distribution of the methane plume [60].
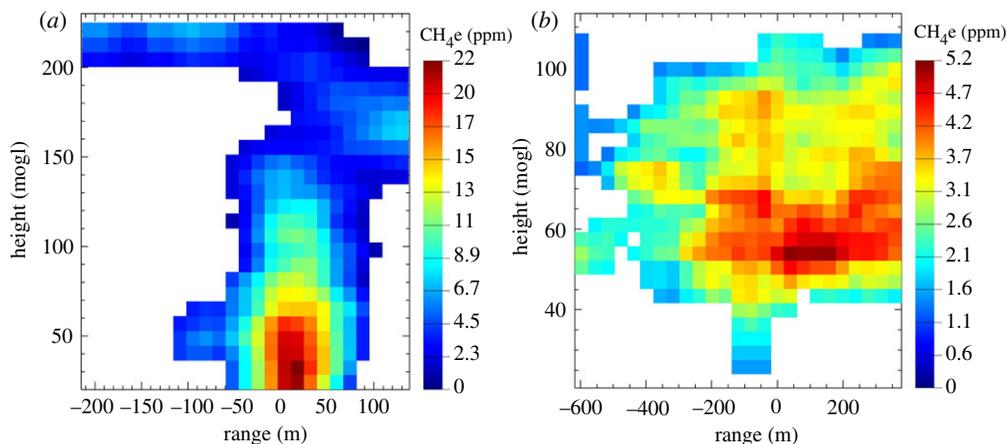
Figure 3. Methane enhancement (CH$_4$e) over background, interpolated onto a two-dimensional flux plane using emission correlations between CO$_2$ measured from a fixed-wing UAV platform and methane at a landfill site in the UK on: (*a*) 27 November 2014; and (*b*) 5 March 2015. Figure taken from Allen *et al.* [40]. (Online version in colour.)
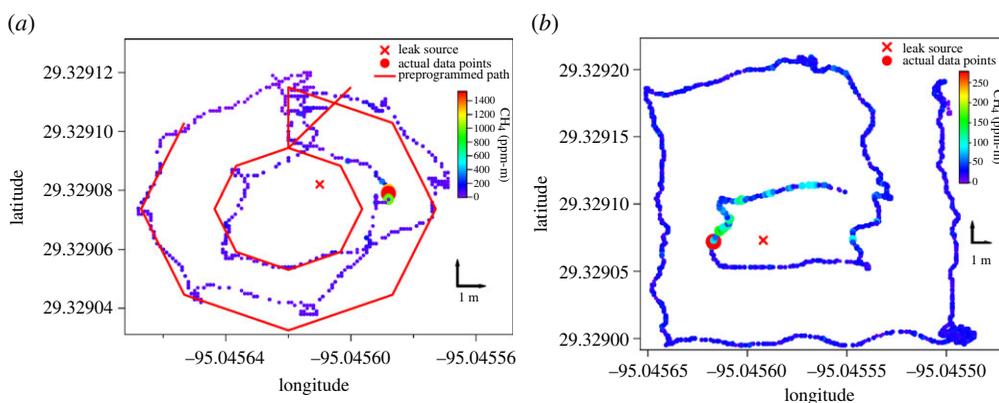

Figure 4. Examples of concentric UAV flight paths are used for estimating the emission rate of target infrastructure via path-integrated methane measurements and the mass balance method [33]. Crosses indicate the location of the leak source, and the colour and size of the data points represent the path-integrated CH$_4$ mixing ratio (ppm-m): (*a*) demonstrates a concentric octagonal flight path and (*b*) demonstrates a concentric rectangular flight path. Figure from Yang *et al.* [33]. (Online version in colour.)

A variant of the mass balance method was used to detect and quantify natural gas leaks using a UAV equipped with a backscatter tunable diode laser absorption spectrometer [33]. This instrument measures path-integrated methane with a sensitivity of 5 ppm-m, equivalent to a 500–5000 ppb methane precision at a near-field distance of 1–10 m. As open-path methane instruments directly measure the total vertical concentration of methane, this removes the need to integrate over the vertical extent of the plume ($\int_{z_1}^{z_2} ([CH_4] - [CH_4]_b)\,dz$). The methane emission flux was estimated from the mean of multiple mass balances performed on concentric paths flown around the target infrastructure at different distances (figure 4). The method tended to underestimate emission fluxes, particularly when the wind speed was low and wind direction variable. Estimated fluxes under the highest wind speeds and steadiest wind direction were approximately 50% accurate. Uncertainty in the GPS location data used in their study also reduced reliability [33].

The mass balance approach, incorporated alongside algorithms to both detect and localize leaks, was used to quantify natural gas emissions using a UAV-based remote sensing measurement platform [87]. Methane measurements were made using an open-path sensor, and quantified fluxes were consistent with those derived using the alternative methodology.

(b) Gaussian plume inversion

Gaussian plume models can be used to model enhancements in methane concentration downwind of a point source using Gaussian statistics [94]. This method has been used for quantifying methane emissions from oil and gas infrastructure using ship-based measurements (e.g. [95,96]), van-based mobile measurements (e.g. [97,98]), and from stationary-site measurements (e.g. [99,100]). The methane flux from a single-point source can be quantified by inverting equation (5.2), which models the downwind methane enhancement as dependant on the methane background, the emission flux rate, the dispersion rate and the wind speed [94].

$$[CH_4](y,z) = \left(\frac{F}{2\pi U_\perp \sigma_y \sigma_z} \times \exp\left(\frac{-y^2}{2\sigma_y^2}\right) \times \left(\exp\left(\frac{-(z-H)^2}{2\sigma_z^2}\right) + \exp\left(\frac{-(z+H)^2}{2\sigma_z^2}\right)\right)\right) + [CH_4]_b,$$

(5.2)

where F is the emission flux, $U_\perp$ is the perpendicular wind speed, H is the height of the emission plume source above the ground and σ_y and σ_z are Gaussian dispersion parameters of the plume in the y (across plume, perpendicular to wind direction) and z (vertical) directions, respectively. It should be noted that for the Gaussian plume method, y is conventionally used to refer to the cross-plume coordinate, whereas x is used to denote the same quantity for the mass balance box method.

Nathan *et al*. [71] used the Gaussian plume method (in conjunction with UAV-based sampling) to compare against methane fluxes derived using the mass balance method. The Gaussian plume method converged to a methane flux of $23\,\mathrm{g\,s^{-1}}$, larger than both the mass balance derived flux ($14 \pm 8\,\mathrm{g\,s^{-1}}$), and the two independent non-UAV-derived fluxes (both $5.8\,\mathrm{g\,s^{-1}}$). Ali *et al*. [86] used the Gaussian plume method and a UAV platform to quantify landfill methane fluxes but were limited by the poor sensitivity of their methane sensor.

The Gaussian plume method usually requires a large amount of time averaging in order for the instantaneous plumes to resolve into an observed Gaussian plume morphology suited to Gaussian inversion. When sampling in close proximity to an emission source (less than approximately 100 m), the time scale of measurements is unlikely to allow for adequate time averaging, and a non-Gaussian distribution of methane may be observed. The turbulent fluctuation of the wind field combined with the short flight duration of many UAVs may result in the measurement of an instantaneous plume and, therefore, a poorly defined plume morphology. However, repeated flights (or longer duration sampling) in less variable wind conditions, combined with carefully designed flight patterns can mitigate this. Individual case studies would need to be evaluated for the conditions specific to the environment at the time of sampling, by comparing data with fitted Gaussian plume assumptions.

A recently developed adaptation of the Gaussian plume flux inversion, referred to as the near-field Gaussian plume inversion (NGI) technique, was adapted for downwind sampling of turbulent plumes close to the emission source [66]. In the NGI method, the methane flux density is calculated at all points across a vertical plane perpendicular to the mean wind direction, using a method similar to that used in the mass balance approach. An emission flux estimate is then derived by fitting the measured methane flux density values to a modelled (Gaussian) flux density, using an adaptation of the two-dimensional Gaussian plume model (equation (2.2)), with the exclusion of wind speed, which is implicitly and spatially accounted for when deriving flux density. A final (optimally fitted) methane emission flux is then calculated by iteratively solving four simultaneous equations, under the assumption that σ_y and σ_z increase linearly with distance
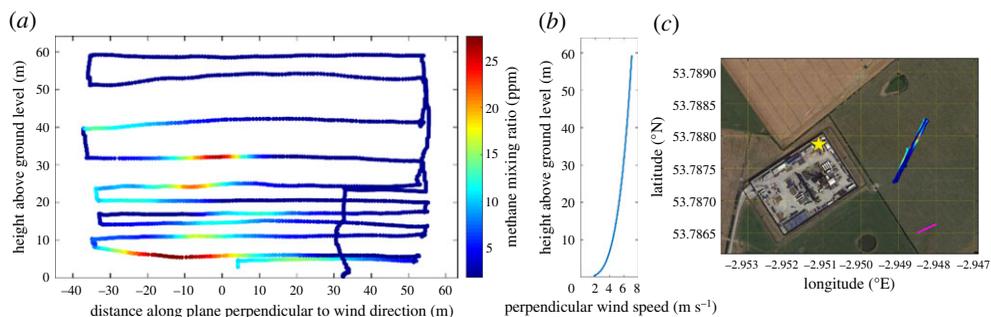
Figure 5. (*a*) Methane mixing ratios (ppm) measured along a UAV flight track showing an example of a geospatially mapped methane plume. Measurements were made on 14 January 2019 at a hydraulic fracturing facility in the UK (see Shah *et al*. [100] for details); (*b*) Perpendicular wind speed measured during sampling using a two-dimensional sonic anemometer mounted on the UAV platform. (*c*) Location of sampling (Google Maps © dated 26 September 2018) showing the UAV flight track. The arrow (bottom right corner) represents the mean wind direction (254.9°) during sampling. Figure taken from Shaw *et al*. [100]. (Online version in colour.)

from the source location (suitable over small distances). This method requires adequate spatial sampling density in both the y and z directions to resolve a flux [66].

Shah *et al*. [38] tested the NGI method using controlled releases of methane. Two rotary-wing UAVs were used: one tethered to a ground-based off-axis ICOS instrument (Los Gatos Research (now ABB) Micro-portable Greenhouse Gas Analyzer), and the second carrying a miniaturized, lighter prototype of the same instrument. The approach was tested for 22 flight surveys, of which 19 produced results with good agreement with the known controlled emission flux. The reported lower ($17 \pm 10\%$) and upper ($227 \pm 98\%$) uncertainty bounds resulted from the variability in the position of instantaneously observed plumes and spatially sparse sampling. While these uncertainties are large, Shah *et al*. [38] concluded that the NGI method is viable in situations where access to an emission source site is prohibited or impractical.

The NGI method was used to quantity the methane emission flux resulting from unintended cold-venting during flowback operations at a hydraulic fracturing facility in the UK [65] (figure 5). In this instance, two UAV platforms were used for methane measurements: a rotary-wing UAV, tethered to a ground-based off-axis ICOS instrument (Los Gatos Research (now ABB) Micro-portable Greenhouse Gas Analyzer) and a second rotary-wing UAV, carrying a miniaturized prototype of the same instrument intended for UAV-based use. Calculated methane fluxes were between 9 and $156 \, \text{g s}^{-1}$, in good agreement with fluxes derived from nearby ground-based monitoring [100]. The range of fluxes derived using the NGI method therefore likely reflects the time-varying nature of the emission source, as well as the derived uncertainty [65].

Another approach related to the Gaussian inversion method was used by Golston *et al*. [87] to quantify methane fluxes from natural gas stations. The method was based on the inverse relationship between methane enhancement and wind speed, and the linear relationship between methane enhancement and emission flow rate (see equation (5.2)), derived from a set of test data. Dispersion in the z direction (σ_z) was accounted for by using an open-path methane sensor measuring column-integrated methane, and dispersion in the y direction (σ_y) was assumed to be small, due to the close proximity to the source. Quantified fluxes were shown to be in agreement with the mass balance approach used in the same study [87].

(c) Alternative approaches

A methane emission flux could feasibly be quantified using UAVs in conjunction with the tracer release method, and a controlled release of a reference tracer gas at a known rate from the source origin (e.g. [92,101–103]). This method removes the problematic need for both meteorological data

Table 2. Summary of advantages and disadvantages for different UAV platforms, sampling methods and flux quantification techniques.

UAV wing type	advantages	disadvantages
fixed-wing UAV	— greater flight speed so can cover a larger spatial area	— require large and open areas free of obstacles for take-off and landing — may require additional apparatus for take-off (e.g. catapult)
rotary-wing UAV	— greater manoeuvrability — vertical take-off and landing capability — easier to control — can hover at a fixed position	— wind speed and wind direction measurements can be more challenging owing to propeller air-flow — adding mass (e.g. instrumentation) away from the centre of gravity can lead to poor flight stability
sampling method	**advantages**	**disadvantages**
air samples collected onboard the UAV	— can use high-precision instrumentation for offline analysis irrespective of mass, size, cost etc. — can measure other variables such as ^{13}C isotopic ratio of methane, or other atmospheric pollutants which can aid source apportionment — full spatial freedom for the UAV platform	— usually results in discretized (snapshot) sampling as opposed to continuous sampling
air sampled through tubing connected to the UAV	— continuous sampling — can use high-precision ground-based instrumentation irrespective of mass, size, cost etc. — could measure other atmospheric variables (e.g. ^{13}C, or other air pollutant)	— must account for the lag-time of the air through the tubing to convolve sampling time with measurement location — limits the range and manoeuvrability of the UAV — the tubing can present physical and logistical challenges, such as snaring, or kinking — weight of tubing increases with sampling height (as more tubing is lifted) reducing flight duration
air sampled live onboard the UAV	— continuous sampling — full spatial freedom for the UAV	— added weight reduces potential flight duration — instrumentation balance between size, weight, cost versus precision, measurement frequency etc.
flux quantification technique*	**advantages**	**disadvantages**
mass balance box model	— can be adapted for either point measurements, or path measurements — can be used for multiple point emission sources, or dispersive emission sources (such as landfill)	— requires dense spatial sampling or some form of interpolation/extrapolation — assumes steady winds
Gaussian plume inversion	— can be adapted for either point measurements, or path measurements	— assumes Gaussian distributed plume (time-averaged)

(*Continued.*)

Table 2. (*Continued*.)

flux quantification technique*	advantages	disadvantages
		— assumes steady winds
		— difficult to adapt for heterogeneous and dispersive emission sources (more suited to singular point emission sources)

*In the context of UAV-based measurements.

and atmospheric modelling of transport and dispersion, but requires instrumentation capable of measuring the tracer gas at high precision in addition to high-precision methane measurements. The tracer release approach relies on the assumption that the co-emitted tracer gas will disperse in the atmosphere in an identical way to that of the methane. In this way, the emission flux of methane can be quantified using the known emission rate of the tracer gas, and the ratio of the tracer gas to methane concentration (above background). To the best of the authors' knowledge, direct use of this method in conjunction with a UAV platform has not yet been made.

Alternative atmospheric inversion approaches could also be applied to UAV-based measurement data to quantify methane fluxes. For example, Lagrangian particle dispersion models simulate the paths of many massless particles as they travel with the local wind field (e.g. [104]) and have been used to quantify methane fluxes (e.g. [100,105]). Lagrangian particle models may be more physically valid than Gaussian inversion approaches, which tend not to model turbulence in the wind, but are computationally more expensive.

Ravikumar *et al.* [106] compared the methane flux quantification capacity of several vehicle, UAV and plane-based technologies but did not present their flux methodology. The accuracy of UAV-based flux quantification, as well as the ratio of positive to negative identification of leaks, was found to be comparable to vehicle-based methods. Ravikumar *et al.* [106] concluded that UAV technologies are still in their infancy, require large amounts of labour and suffer from regular battery changes and frequent groundings during adverse conditions. Despite this, their capability for quantifying emissions from tall infrastructure, and during calmer atmospheric conditions, was noted as being particularly advantageous relative to vehicle-based monitoring.

6. Conclusion

The literature reviewed here demonstrates the clear capability of small UAV-based measurement platforms for quantifying methane fluxes from a range of sources at local scales (less than 1 km). Such capability has only become available over the past decade, as a result of advances in both UAV technology and the miniaturization of instrumentation for the measurement of methane. Lightweight and high-performance instrumentation, with the capacity to measure methane with a precision on the order of a few ppb, are now becoming commercially available (at the time of writing), and developments continue to be made at pace. Such instrumentation will enable more accurate flux quantification, particularly of smaller emission sources which may not be captured by current methodology. Further developments in UAV technology would also be highly beneficial. Enhanced flight duration, as a result of improved battery capacity, would be extremely advantageous in terms of plume mapping, allowing for extended temporal ranges and refined spatial resolution of methane measurements. A summary of advantages and disadvantages of different UAV platform types, sampling methodologies, and flux quantification techniques is presented in table 2.

UAVs provide a highly versatile platform, uniquely suited for high-density spatial mapping of methane plumes, and quantifying methane emissions at local scales. Their use could easily be incorporated into policy and regulation concerning monitoring and quantification of methane emissions from polluting industries [53] and also offer potential applications in hazard

assessment (natural gas leaks), and extension to other emissions of interest, such as air quality pollutants.

References

1. Dlugokencky E. 2021 NOAA/ESRL. www.esrl.noaa.gov/gmd/ccgg/trends_ch4 (accessed February 2021).

2. Nisbet EG *et al.* 2019 Very strong atmospheric methane growth in the 4 years 2014–2017: implications for the Paris Agreement. *Glob. Biogeochem. Cy.* **33**, 318–342. (doi:10.1029/2018GB006009)

3. Ganesan AL *et al.* 2019 Advancing scientific understanding of the global methane budget in support of the Paris Agreement. *Glob. Biogeochem. Cy.* **33**, 1475–1512. (doi:10.1029/2018GB006065)

4. Saunois M *et al.* 2020 The global methane budget 2000–2017. *Earth Syst. Sci. Data* **12**, 1561–1623. (doi:10.5194/essd-12-1561-2020)

5. Dlugokencky EJ, Steele LP, Lang PM, Masarie KA. 1994 The growth rate and distribution of atmospheric methane. *J. Geophys. Res. Atmos.* **99**, 17 021–17 043. (doi:10.1029/94JD01245)

6. Karion A *et al.* 2013 Methane emissions estimate from airborne measurements over a western United States natural gas field. *Geophys. Res. Lett.* **40**, 4393–4397. (doi:10.1002/grl.50811)

7. O'Shea SJ, Bauguitte SJ-B, Gallagher MW, Lowry D, Percival CJ. 2013 Development of a cavity-enhanced absorption spectrometer for airborne measurements of CH_4 and CO_2. *Atmos. Meas. Tech.* **6**, 1095–1109. (doi:10.5194/amt-6-1095-2013)

8. Cambaliza MO *et al.* 2014 Assessment of uncertainties of an aircraft-based mass balance approach for quantifying urban greenhouse gas emissions. *Atmos. Chem. Phys.* **14**, 9020–9050. (doi:10.5194/acp-14-9029-2014)

9. Pitt JR *et al.* 2016 The development and evaluation of airborne in situ N_2O and CH_4 sampling using a quantum cascade laser absorption spectrometer. *Atmos. Meas. Tech.* **9**, 63–77. (doi:10.5194/amt-9-63-2016)

10. Klausner T *et al.* 2020 Urban greenhouse gas emissions from the Berlin area: a case study using airborne CO_2 and CH_4 in situ observations in summer 2018. *Elem. Sci. Anth.* **8**, 15. (doi:10.1525/elementa.411)

11. Hu H, Landgraf J, Detmers R, Borsdorff T, de Brugh JA, Aben I, Butz A, Hasekamp O. 2018 Toward global mapping of methane with TROPOMI: first results and intersatellite comparison to GOSAT. *Geophys. Res. Lett.* **45**, 3682–3689. (doi:10.1002/2018GL077259)

12. Sheng JX, Jacob DJ, Maasakkers JD, Zhang Y, Sulprizio MP. 2018 Comparative analysis of low-Earth orbit (TROPOMI) and geostationary (GeoCARB, GEO-CAPE) satellite instruments for constraining methane emissions on fine regional scales: application to the Southeast US. *Atmos. Meas. Tech.* **11**, 6379–6388. (doi:10.5194/amt-11-6379-2018)

13. Lorente A *et al.* 2021 Methane retrieved from TROPOMI: improvement of the data product and validation of the first two years of measurements. *Atmos. Meas. Tech.* **14**, 665–684. (doi:10.5194/amt-14-665-2021)

14. Knox SH *et al.* 2019 FLUXNET-CH4 synthesis activity: objectives, observations and future directions. *B. Am. Meteorol. Soc.* **100**, 2607–2632. (doi:10.1175/BAMS-D-18-0268.1)

15. Shaw JT *et al.* 2019 A baseline of atmospheric greenhouse gases for prospective UK shale gas sites. *Sci. Tot. Env.* **684**, 1–13. (doi:10.1016/j.scitotenv.2019.05.266)

16. Zazzeri G, Lowry D, Fisher RE, France JL, Lanoisellé M, Nisbet EG. 2015 Plume mapping and isotopic characterisation of anthropogenic methane sources. *Atmos. Environ.* **110**, 151–162. (doi:10.1016/j.atmosenv.2015.03.029)

17. Von Fischer JC *et al.* 2017 Rapid, vehicle-based identification of location and magnitude of urban natural gas pipeline leaks. *Environ. Sci. Technol.* **51**, 4091–4099. (doi:10.1021/acs.est.6b06095)

18. Lowry D *et al.* 2020. Environmental baseline monitoring for shale gas development in the UK: identification and geochemical characterisation of local source emissions of methane to atmosphere. *Sci. Tot. Env.* **708**, 134600. (doi:10.1016/j.scitotenv.2019.134600)

19. O'Shea SJ *et al.* 2014 Methane and carbon dioxide fluxes and their regional scalability for the European Arctic wetlands during the MAMM project in summer 2012. *Atmos. Chem. Phys.* **14**, 13 159–13 174. (doi:10.5194/acp-14-13159-2014)

20. Pitt JR, Allen G, Bauguitte SJB, Gallagher MW, Lee JD, Drysdale W, Nelson B, Manning AJ, Palmer PI. 2019 Assessing London CO_2, CH_4, and CO emissions using aircraft measurements and dispersion modelling. *Atmos. Chem. Phys.* **19**, 8931–8945. (doi:10.5194/acp-19-8931-2019)

21. Fiehn A *et al.* 2020 Estimating CH_4, CO_2 and CO emissions from coal mining and industrial activities in the Upper Silesian Coal Basin using an aircraft-based mass balance approach. *Atmos. Chem. Phys.* **20**, 12 675–12 695. (doi:10.5194/acp-20-12675-2020)

22. Lee JD *et al.* 2018 Flow rate and source reservoir identification from airborne chemical sampling of the uncontrolled Elgin platform gas release. *Atmos. Meas. Tech.* **11**, 1725–1739. (doi:10.5194/amt-11-1725-2018)

23. France JL *et al.* 2021 Facility level measurement of offshore oil and gas installations from a medium-sized airborne platform: method development for quantification and source identification of methane emissions. *Atmos. Meas. Tech.* **14**, 71–88. (doi:10.5194/amt-14-71-2021)

24. Caulton DR *et al.* 2014 Toward a better understanding and quantification of methane emissions from gas development. *Proc. Natl Acad. Sci. USA* **111**, 6237–6242. (doi:10.1073/pnas.1316546111)

25. Illingworth S *et al.* 2014 Measurements of boundary layer ozone concentrations on-board a Skywalker unmanned aerial vehicle. *Atmos. Sci. Lett.* **15**, 252–258. (doi:10.1002/asl2.496)

26. Villa TF, Gonzalez F, Miljievic B, Ristovski ZD, Morawska L. 2016 An overview of small unmanned aerial vehicles for air quality measurements: present applications and future prospectives. *Sensor-Basel* **16**, 1072. (doi:10.3390/s16071072)

27. Nolan PJ *et al.* 2018 Coordinated unmanned aircraft system (UAS) and ground-based weather measurements to predict Lagrangian coherent structures (LCSs). *Sensors-Basel* **18**, 4448. (doi:10.3390/s18124448)

28. Schuyler TJ, Gohari SMI, Pundsack G, Berchoff D, Guzman MI. 2019 Using a balloon-launched unmanned glider to validate real-time WRF modelling. *Sensors* **19**, 1914. (doi:10.3390/s19081914)

29. Connor D, Martin PG, Scott TB. 2016 Airborne radiation mapping: overview and application of current and future aerial systems. *Int. J. Remote Sens.* **37**, 5953–5987. (doi:10.1080/01431161.2016.1252474)

30. James MR *et al.* 2020 Volcanological applications of unoccupied aircraft systems (UAS): developments, strategies, and future challenges. *Volcanica* **3**, 67–114. (doi:10.30909/vol.03.01.67114)

31. Watts AC, Ambrosia VG, Hinkley EA. 2012 Unmanned aircraft systems in remote sensing and scientific research: classification and considerations of use. *Remote Sens.* **4**, 1671–1692. (doi:10.3390/rs4061671)

32. Schuyler TJ, Guzman MI. 2017 Unmanned aerial systems for monitoring trace tropospheric gases. *Atmosphere-Basel* **8**, 206. (doi:10.3390/atmos8100206)

33. Yang S, Talbot RW, Frish MB, Golston LM, Aubut NF, Zondlo MA, Gretencord C, McSpiritt J. 2018 Natural gas fugitive leak detection using an unmanned aerial vehicle: measurement system description and mass balance approach. *Atmosphere* **9**, 383. (doi:10.3390/atmos9100383)

34. Brosy C, Krampf K, Zeeman M, Wolf B, Junkermann W, Schäfer K, Emeis S, Kuntsmann H. 2017 Simultaneous multicopter-based air sampling and sensing of meteorological variables. *Atmos. Meas. Tech.* **10**, 2773–2784. (doi:10.5194/amt-10-2773-2017)

35. Oberle FKJ, Gibbs AE, Richmond BM, Erikson LH, Waldrop MP, Swarzenski PW. 2019 Towards determining spatial methane distribution on Arctic permafrost bluffs with an unmanned aerial system. *SN Appl. Sci.* **1**, 236. (doi:10.1007/s42452-019-0242-9)

36. Chang CC, Wang JL, Chang CY, Liang MC, Lin MR. 2016 Development of a multi-copter-carried whole air sampling apparatus and its applications in environmental studies. *Chemosphere* **144**, 484–492. (doi:10.1016/j.chemosphere.2015.08.028)

37. Emran BJ, Tannant DD, Najjaran H. 2017 Low-altitude aerial methane concentration mapping. *Remote Sens.* **9**, 823. (doi:10.3390/rs9080823)

38. Shah A, Pitt JR, Ricketts H, Leen JB, Williams PI, Kabbabe K, Gallagher MW, Allen G. 2020 Testing the near-field Gaussian plume inversion flux quantification technique using unmanned aerial vehicle sampling. *Atmos. Meas. Tech.* **13**, 1467–1484. (doi:10.5194/amt-13-1467-2020)

39. Khan A, Schaefer D, Tao L, Miller DJ, Sun K, Zondlo MA, Harrison WA, Roscoe B, Lary DJ. 2012 Low power greenhouse gas sensors for unmanned aerial vehicles. *Remote Sens.* **4**, 1355–1368. (doi:10.3390/rs4051355)

40. Allen G *et al.* 2019 The development and trial of an unmanned aerial system for the measurement of methane flux from landfill and greenhouse gas emission hotspots. *Waste Manage.* **87**, 883–892. (doi:10.1016/j.wasman.2017.12.024)

41. Van den Kroonenberg A, Martin T, Buschmann M, Bange J, Vörsmann P. 2008 Measuring the wind vector using the autonomous mini aerial vehicle M2AV. *J. Atmos. Ocean. Tech.* **25**, 1969–1982. (doi:10.1175/2008JTECHA1114.1)

42. Wildmann N, Hofsäß M, Weimer F, Joos A, Bange J. 2014 MASC – A small remotely piloted aircraft (RPA) for wind energy research. *Adv. Sci. Res.* **11**, 55–61. (doi:10.5194/asr-11-55-2014)

43. Witte BM, Singler RF, Bailey SCC. 2017 Development of an unmanned aerial vehicle for the measurement of turbulence in the atmospheric boundary layer. *Atmosphere-Basel* **8**, 195. (doi:10.3390/atmos8100195)

44. de Jong R, Chor T, Dias N. 2011 Medição de velocidade do vento a bordo de um Veículo Aéreo Não Tripulado. *Ciênc. Nat.* **33**, 71–74.

45. Niedzielski T *et al.* 2017 Are estimates of wind characteristics based on measurements with Pitot tubes and GNSS receivers mounted on consumer-grade unmanned aerial vehicles applicable in meteorological studies? *Environ. Monit. Assess.* **189**, 431. (doi:10.1007/s10661-017-6141-x)

46. Mayer S, Hattenberger G, Brisset P, Jonassen M, Reuder J. 2012 A 'no-flow-sensor' wind estimation algorithm for unmanned aerial systems. *Int. J. Micro. Air Veh.* **4**, 15–30. (doi:10.1260%2F1756-8293.4.1.15)

47. Bonin T, Chilson P, Zielke B, Klein P, Leeman J. 2013 Comparison and application of wind retrieval algorithms for small unmanned aerial systems. *Geosci. Instrum. Methods Data Syst.* **2**, 177–187. (doi:10.5194/gi-2-177-2013)

48. Elston J, Argrow B, Stachura M, Weibel D, Lawrence D, Pope D. 2015 Overview of small fixed-wing unmanned aircraft for meteorological sampling. *J. Atmos. Ocean. Tech.* **32**, 97–115. (doi:10.1175/JTECH-D-13-00236.1)

49. Rautenberg A, Graf MS, Wildmann N, Platis A, Bange J. 2018 Reviewing wind measurement approaches for fixed-wing unmanned aircraft. *Atmosphere-Basel* **9**, 422. (doi:10.3390/atmos9110422)

50. Neumann PP, Bartholmai M. 2015 Real-time wind estimation on a micro unmanned aerial vehicle using its inertial measurement unit. *Sens. Actuators A Phys.* **235**, 300–310. (doi:10.1016/j.sna.2015.09.036)

51. Palomaki RT, Rose NT, van den Bossche M, Sherman TJ, de Wekker SF. 2017 Wind estimation in the lower atmosphere using multirotor aircraft. *J. Atmos. Ocean. Technol.* **34**, 1183–1191. (doi:10.1175/JTECH-D-16-0177.1)

52. Barbieri L *et al.* 2019 Intercomparison of small unmanned aircraft system (sUAS) measurements for atmospheric science during the LAPSE-RATE campaign. *Sensor* **19**, 2179. (doi:10.3390/s19092179)

53. Allen G, Gallagher M, Hollingsworth P, Illingworth S, Kabbabe K, Percival C. 2014 *Feasibility of aerial measurements of methane from landfill.* Report – SC130034/R. Bristol, UK: Environment Agency.

54. Burgués J, Marco S. 2020 Environmental chemical sensing using small drones: a review. *Sci. Tot. Env.* **748**, 141172. (doi:10.1016/j.scitotenv.2020.141172)

55. Hodgkinson J, Tatam RP. 2013 Optical gas sensing: a review. *Meas. Sci. Technol.* **24**, 012004. (doi:10.1088/0957-0233/24/1/012004)

56. Fox TA, Barchyn TE, Risk D, Ravikumar AP, Hugenholtz C. 2019 A review of close-range and screening technologies for mitigating fugitive methane emissions in upstream oil and gas. *Environ. Res. Lett.* **14**, 053002. (doi:10.1088/1748-9326/ab0cc3)

57. Mønster J, Kjeldsen P, Scheutz C. 2019 Methodologies for measuring fugitive methane emissions from landfills – A review. *Waste Manage.* **87**, 835–859. (doi:10.1016/j.wasman.2018.12.047)

58. Wang F, Jia S, Wang Y, Tang Z. 2019 Recent developments in modulation spectroscopy for methane detection based on tunable diode laser. *Appl. Sci.* **9**, 2816. (doi:10.3390/app9142816)

59. Takriti M, Wynn PM, Elias DMO, Ward SE, Oakley S, McNamara NP. 2021 Mobile methane measurements: effects of instrument specifications on data interpretation, reproducibility, and isotopic precision. *Atmos. Environ.* **246**, 118067. (doi:10.1016/j.atmosenv.2020.118067)

60. Shah A. 2020 Methane flux quantification using unmanned aerial vehicles. PhD thesis, University of Manchester, UK.

61. Brownlow R *et al.* 2016 Methane mole fraction and δ^{13}C above and below the trade wind inversion at Ascension Island in air sampled by aerial robotics. *Geophys. Res. Lett.* **43**, 11 893–11 902. (doi:10.1002/2016GL071155)

62. Greatwood C, Richardson TS, Freer J, Thomas RM, MacKenzie AR, Brownlow R, Lowry D, Fisher RE, Nisbet EG. 2017 Atmospheric sampling on Ascension Island using multirotor UAVs. *Sensors-Basel* **17**, 1189. (doi:10.3390/s17061189)

63. Andersen T, Scheeren B, Peters W, Chen H. 2018 A UAV-based active AirCore system for measurements of greenhouse gases. *Atmos. Meas. Tech.* **11**, 2683–2699. (doi:10.5194/amt-11-2683-2018)

64. Chang CC, Chang CY, Wang JL, Pan XX, Chen YC, Ho YJ. 2020 An optimized multicopter UAV sounding technique (MUST) for probing comprehensive atmospheric variables. *Chemosphere* **254**, 126867. (doi:10.1016/j.chemosphere.2020.126867)

65. Shah A, Ricketts H, Pitt JR, Shaw JT, Kabbabe K, Leen JB, Allen G. 2020 Unmanned aerial vehicle observations of cold venting from exploratory hydraulic fracturing in the United Kingdom. *Environ. Res. Commun.* **2**, 021003. (doi:10.1088/2515-7620/ab716d)

66. Shah A *et al.* 2019 A near-field Gaussian plume inversion flux quantification method, applied to unmanned aerial vehicle sampling. *Atmosphere* **10**, 396. (doi:10.3390/atmos10070396)

67. Shah A, Pitt J, Kabbabe K, Allen G. 2019 Suitability of a non-dispersive infrared methane sensor package for flux quantification using an unmanned aerial vehicle. *Sensors* **19**, 4705. (doi:10.3390/s19214705)

68. Gardiner T, Mead MI, Garcelon S, Robinson R, Swann N, Hansford GM, Woods PT, Jones RL. 2010 A lightweight near-infrared spectrometer for the detection of trace atmospheric species. *Rev. Sci. Instrum.* **81**, 083102. (doi:10.1063/1.3455827)

69. Frish MB *et al.* 2013 *Low-cost lightweight airborne laser-based sensors for pipeline leak detection and reporting.* In Proc. Spie. 87260C.

70. Golston LM *et al.* 2017 Lightweight mid-infrared methane sensor for unmanned aerial systems. *Appl. Phys. B-Lasers O.* **123**, 170. (doi:10.1007/s00340-017-6735-6)

71. Nathan BJ *et al.* 2015 Near-field characterization of methane emission variability from a compressor station using a model aircraft. *Environ. Sci. Technol.* **49**, 7896–7903. (doi:10.1021/acs.est.5b00705)

72. Smith BJ, John G, Christensen LE, Chen YQ. 2017 Fugitive methane leak detection using sUAS and miniature laser spectrometer payload: system application and groundtruthing tests. In *2017 Int. Conf. on Unmanned Aircraft Systems (ICUAS)*, pp. 369–374. Piscataway, NJ: IEEE.

73. Barchyn TE, Hugenholtz CH, Myshak S, Bauer J. 2018 A UAV-based system for detecting natural gas leaks. *J. Unmanned Veh. Syst.* **6**, 18–30. (doi:10.1139/juvs-2017-0018)

74. Barchyn TE, Hugenholtz CH, Fox TA. 2019 Plume detection modelling of a drone-based natural gas leak detection system. *Elem. Sci. Anth.* **7**, 41. (doi:10.1525/elementa.379)

75. Cossel KC *et al.* 2017 Open-path dual-comb spectroscopy to an airborne retroreflector. *Optica* **4**, 724–728. (doi:10.1364/OPTICA.4.000724)

76. Berman ESF, Fladeland M, Liem J, Kolyer R, Gupta M. 2012 Greenhouse gas analyser for measurements of carbon dioxide, methane, and water vapor aboard an unmanned aerial vehicle. *Sensor Actuat. B-Chem.* **169**, 128–135. (doi:10.1016/j.snb.2012.04.036)

77. Martinez B, Miller TW, Yalin AP. 2020 Cavity ring-down methane sensor for small unmanned aerial systems. *Sensors* **20**, 454. (doi:10.3390/s20020454)

78. Tratt DM, Buckland KN, Hall JL, Johnson PD, Keim ER, Leifer I, Westberg K, Young SJ. 2014 Airborne visualization and quantification of discrete methane sources in the environment. *Proc. Spie.* **154**, 74–88. (doi:10.1016/j.rse.2014.08.011)

79. Lehmann JRK, Münchberger W, Knoth C, Blodau C, Nieberding F, Prinz T, Pancotto VA, Kleinebecker T. 2016 High-resolution classification of South Patagonian peat bog microforms reveals potential gaps in upscaled CH_4 fluxes by use of an unmanned aerial system (UAS) and CIR imagery. *Remote Sens.* **8**, 173. (doi:10.3390/rs8030173)

80. Tanda G, Migliazzi M, Chiarabini V, Cinquetti P. 2017 Application of close-range aerial infrared thermography to detect landfill gas emissions: a case study. *J. Phys.* **796**, 012016. (doi:10.1088/1742-6596/796/1/012016)

81. Fjelsted L, Christensen AG, Larsen JE, Kjeldsen P, Scheutz C. 2019 Assessment of a landfill methane emission screening method using an unmanned aerial vehicle mounted thermal infrared camera – A field study. *Waste Manage.* **87**, 893–904. (doi:10.1016/j.wasman.2018.05.031)

82. Daugéla I, Visockiene JS, Kumpiene J. 2020 Detection and analysis of methane emissions from a landfill using unmanned aerial drone systems and semiconductor sensors. *Detritus* **10**, 127–138. (doi:10.31025/2611-4135/2020.13942)

83. Kanan SM, El-Kadri OM, Abu-Yousef IA, Kanan MC. 2009 Semiconducting metal oxide based sensors for selective gas pollution detection. *Sensors* **9**, 8158–8196. (doi:10.3390/s91008158)

84. Aldhafeeri T, Tran MK, Vrolyk R, Pope M, Fowler M. 2020 A review of methane gas detection sensors: recent developments and future perspectives. *Inventions* **5**, 28. (doi:10.3390/inventions5030028)

85. Taguem EM, Romain A-C. 2019 MOS sensors array for methane monitoring with UAS. In *IEEE Int. Sym. on Olfaction and Electronic Nose*. Piscataway, NJ: IEEE.

86. Ali NBH, Abichou T, Green R. 2020 Comparing estimates of fugitive landfill methane emissions using inverse plume modelling obtained with Surface Emission Monitoring (SEM), Drone Emission Monitoring (DEM), and Downwind Plume Emission Monitoring (DWPEM). *J. Air Waste Manag. Assoc.* **70**, 410–424. (doi:10.1080/10962247.2020.1728423)

87. Golston LM, Aubut NF, Frish MB, Yang S, Talbot RW, Gretencord C, McSpiritt J, Zondlo MA. 2018 Natural gas fugitive leak detection using an unmanned aerial vehicle: localization and quantification of emission rate. *Atmosphere* **9**, 333. (doi:10.3390/atmos9090333)

88. Heimburger A *et al.* 2017 Assessing the optimised precision of the aircraft mass balance method for measurement of urban greenhouse gas emission rates through averaging. *Elem. Sci. Anth.* **5**, 26. (doi:10.1525/elementa.134)

89. White WH, Anderson JA, Blumenthal DL, Husar RB, Gillani NV, Husar JD, Wilson Jr WE. 1976 Formation and transport of secondary air pollutants: ozone and aerosols in the St. Louis urban plume. *Science* **194**, 187–189. (doi:10.1126/science.959846)

90. O'Shea SJ, Allen G, Fleming ZL, Bauguitte SJB, Percival CJ, Gallagher MW, Lee J, Helfter C, Nemitz E. 2014 Area fluxes of carbon dioxide, methane, and carbon monoxide derived from airborne measurements around Greater London: a case study during summer 2012. *J. Geophys. Res. Atmos.* **119**, 4940–4952. (doi:10.1002/2013JD021269)

91. Baer DS, Paul JB, Gupta M, O'Keefe A. 2002 Sensitive absorption measurements in the near-infrared region using off-axis integrated-cavity-output spectroscopy. *Appl. Phys. B.* **75**, 261–265. (doi:10.1007/s00340-002-0971-z)

92. Scheutz C, Samuelsson J, Fredenslund AM, Kjeldsen P. 2011 Quantification of multiple methane emission sources at landfills using a double tracer technique. *Waste Manage.* **31**, 1009–1017. (doi:10.1016/j.wasman.2011.01.015)

93. Mays KL, Shepson PB, Stirm BH, Karion A, Sweeney C, Gurney KR. 2009 Aircraft-based measurements of the carbon footprint of Indianapolis. *Environ. Sci. Technol.* **43**, 7816–7823. (doi:10.1021/es901326b)

94. Turner DB. 1994 Estimates of atmospheric dispersion. In *Workbook of atmospheric dispersion estimates: an introduction to dispersion modeling* (ed. DB Turner), 2nd edn. Boca Raton, FL: CRC Press, Inc.

95. Riddick SN *et al.* 2019 Methane emissions from oil and gas platforms in the North Sea. *Atmos. Chem. Phys.* **19**, 9787–9796. (doi:10.5194/acp-19-9787-2019)

96. Yacovitch TI, Daube C, Herndon SC. 2020 Methane emissions from offshore oil and gas platforms in the Gulf of Mexico. *Environ. Sci. Technol.* **54**, 3530–3538. (doi:10.1021/acs.est.9b07148)

97. Rella CW, Tsai TR, Botkin CG, Crosson ER, Steele D. 2015 Measuring emissions from oil and natural gas well pads using the mobile flux plane technique. *Environ. Sci. Technol.* **49**, 4742–4748. (doi:10.1021/acs.est.5b00099)

98. Bell CS *et al.* 2017 Comparison of methane emission estimates from multiple measurement techniques at natural gas production pads. *Elem Sci. Anthrop.* **5**, 79. (doi:10.1525/elementa.266)

99. Foster-Wittig TA, Thoma ED, Albertson JD. 2015 Estimation of point source fugitive emission rates from a single sensor time series: a conditionally-sampled Gaussian plume reconstruction. *Atmos. Environ.* **115**, 101–109. (doi:10.1016/j.atmosenv.2015.05.042)

100. Shaw JT *et al.* 2020 Methane flux from flowback operations at a shale gas site. *JAPCA J. Air Waste Manag.* **70**, 1324–1339. (doi:10.1080/10962247.2020.1811800)

101. Scheutz C, Kjeldsen P, Bogner JE, de Visscher A, Gerbert J, Hilger HA, Huber-Humer M, Spokas K. 2009 Microbial methane oxidation processes and technologies for mitigation of landfill gas emissions. *Waste Manag. Res.* **27**, 409–455. (doi:10.1177/0734242X09339325)

102. Mønster JG, Samuelsson J, Kjedlsen P, Rella CW, Scheutz C. 2014 Quantifying methane emission from fugitive sources by combining tracer release and downwind measurements – A sensitivity analysis based on multiple field surveys. *Waste Manage.* **34**, 1416–1428. (doi:10.1016/j.wasman.2014.03.025)

103. Mønster JG, Samuelsson J, Kjedlsen P, Scheutz C. 2015 Quantification of methane emissions from 15 Danish landfills using the mobile tracer dispersion method. *Waste Manage.* **35**, 177–186. (doi:10.1016/j.wasman.2014.09.006)

104. Flesch TK, Wilson JD, Yee E. 1995 Backward-time Lagrangian stochastic dispersion models, and their application to estimate gaseous emissions. *J. Appl. Meteor.* **34**, 1320–1332. (doi:10.1175/1520-0450(1995)034%3C1320:BTLSDM%3E2.0.CO;2)

105. Riddick SN *et al.* 2017 Estimating the size of a methane emission point source at different scales: from local to landscape. *Atmos. Chem. Phys.* **17**, 7839–7851. (doi:10.5194/acp-17-7839-2017)

106. Ravikumar AP *et al.* 2019 Single-blind intercomparison of methane detection technologies – Results from the Stanford/EDF mobile monitoring challenge. *Elem. Sci. Anth.* **7**, 37. (doi:10.1525/elementa.373)